The Astrophysical Journal Letters, 802:L1 (6pp), 2015 March 20 doi:10.1088/2041-8205/802/1/L1

EVIDENCE OF CROSS-CORRELATION BETWEEN THE CMB LENSING AND THE γ-RAY SKY

Nicolao Fornengo[1,2], Laurence Perotto[3], Marco Regis[1,2], and Stefano Camera[4,5]
[1] Dipartimento di Fisica, Università di Torino, I-10125 Torino, Italy; regis@to.infn.it
[2] Istituto Nazionale di Fisica Nucleare, Sezione di Torino, I-10125 Torino, Italy
[3] LPSC, Université Grenoble-Alpes, CNRS/IN2P3, 53, rue des Martyrs, F-38026 Grenoble Cedex, France
[4] Jodrell Bank Centre for Astrophysics, The University of Manchester, Manchester M13 9PL, UK
[5] CENTRA, Instituto Superior Técnico, Universidade de Lisboa, Lisboa, Portugal
Received 2014 December 23; accepted 2015 February 25; published 2015 March 16

ABSTRACT

We report the measurement of the angular power spectrum of cross-correlation between the unresolved component of the *Fermi*-LAT γ-ray sky maps and the cosmic microwave background lensing potential map reconstructed by the *Planck* satellite. The matter distribution in the universe determines the bending of light coming from the last scattering surface. At the same time, the matter density drives the growth history of astrophysical objects, including their capability at generating non-thermal phenomena, which in turn give rise to γ-ray emissions. The *Planck* lensing map provides information on the integrated distribution of matter, while the integrated history of γ-ray emitters is imprinted in the *Fermi*-LAT sky maps. We report here the first evidence of their correlation. We find that the multipole dependence of the cross-correlation measurement is in agreement with current models of the γ-ray luminosity function for active galactic nuclei and star-forming galaxies, with a statistical evidence of 3.0σ. Moreover, its amplitude can in general be matched only assuming that these extragalactic emitters are also the bulk contribution of the measured isotopic γ-ray background (IGRB) intensity. This leaves little room for a big contribution from galactic sources to the IGRB measured by *Fermi*-LAT, pointing toward direct evidence of the extragalactic origin of the IGRB.

Key words: gamma rays: diffuse background – gravitational lensing: weak – large-scale structure of universe

Supporting material: data behind figure

1. INTRODUCTION

The weak gravitational lensing by large-scale structures imprints the integrated dark matter distribution onto the cosmic microwave background (CMB) anisotropies. It results in a remapping of the CMB observables, which depends on the line-of-sight integral of the gravitational potential, with a broad kernel peaking at a redshift $z \sim 2$, and which is referred to as the lensing potential (Blanchard & Schneider 1987; see also Lewis & Challinor 2006 for a review). This process perturbates the statistical properties of the CMB observables, which are primarily very close to Gaussian fields. This non-Gaussian signature can be exploited to extract the lensing potential from the CMB maps (Okamoto & Hu 2003). Using such a technique, the *Planck* Collaboration obtained nearly all-sky maps of the lensing potential reconstructed from an undusted CMB temperature map (Planck Collaboration et al. 2014a) and from both foreground-cleaned CMB temperature and polarization maps (Planck Collaboration et al. 2015). They provide us with an estimate of the matter distribution, mainly sensitive to halos located at $1 \lesssim z \lesssim 3$.

On the other hand, the accretion of baryonic matter in halos also creates active astrophysical objects. They can host violent phenomena, such as, e.g., supernova explosions and relativistic outflows, which are able to accelerate particles to high energies. Particles with GeV–TeV energy interacting with the ambient medium emit γ-ray radiation, mostly by means of production and decay of neutral pions, inverse Compton scattering, and non-thermal bremsstrahlung. In addition, the same dark matter that forms the halos could produce γ-rays through its self-annihilation or decay. In the past few decades, the all-sky diffuse γ-ray emission has been measured, but its origin and composition remain key open questions in high-energy astrophysics. The featureless energy spectrum of the isotropic γ-ray background (IGRB; Fermi-LAT Collaboration et al. 2010, 2014) and its flat angular power spectrum (APS; Fermi-LAT Collaboration et al. 2012a) make the IGRB identification a complex task. The cross-correlation of the IGRB with large-scale structure tracers is a very valuable technique for understanding its composition (Xia et al. 2011; Camera et al. 2013; Ando 2014; Ando et al. 2014; Fornengo & Regis 2014; Shirasaki et al. 2014).

In this work, we first show that the lensing potential map estimated by *Planck* and the γ-ray sky observed by *Fermi*-LAT do correlate, by reporting a measurement of their cross-correlation APS. This stems from their common origin associated with extragalactic structures, and we discuss the extragalactic γ-ray background (EGB) properties that can explain the measurement.

The adopted cosmological model throughout this paper is the six-parameter ΛCDM *Planck* best-fitting model reported in Planck Collaboration et al. (2014a).

2. DATA AND ANALYSIS

We use the γ-ray measurements obtained by the *Fermi*-LAT in its first 68 months of operation, from early 2008 August to late 2014 April. We have processed the data with the Fermi Science Tools version `v9r32p5`, using the Pass7-reprocessed instrument response functions for the CLEAN event class (P7REP CLEAN V15) for both the FRONT and BACK conversion types of events, which have been taken together. We have selected photon counts from 700 MeV to 300 GeV, subdivided into 70 energy bins (uniform in log scale) and mapped with a pixel size of $0.^{\circ}125$ (suitable for subsequent HEALPIX projection with $N_{\rm side} = 512$). The *Fermi*-LAT exposure maps

have been derived on the same energy grid and resolution, and we adopted a step size $\cos\theta = 0.025$ in order to have sufficiently refined exposures. From the count and exposure map cubes, we have finally derived the full-sky flux maps. For the cross-correlation analysis, we have grouped the energy sections in six bins (with boundaries at 0.7, 0.99, 2.0, 5.1, 10.2, 48.7, and 300 GeV).

The maps are contaminated by the galactic foreground: since we are interested in the extragalactic signal only, the maps have been cleaned by subtracting the *Fermi*-LAT galactic model `gll_iem_v05`, which can be obtained from the *Fermi*-LAT website.[6]

We account for *Fermi*-LAT point-spread function attenuation (which can be relevant at the angular scales of interest) by correcting the measured APS through a beam window function built as described in Fermi-LAT Collaboration et al. (2012a).

As part of its public data releases of 2015 (2013), the *Planck* Collaboration provided a CMB lensing convergence (potential) map that was employed in our analysis. We use the convergence harmonic coefficients $\kappa_{\ell m} = \ell(\ell+1)/2\,\phi_{\ell m}$ instead of the potential ϕ to reduce the steepness of the APS as a function of multipoles. The methodology followed to derive a convergence map from the 2013 potential map is described in Planck Collaboration et al. (2014b).

We then mask regions contaminated by galactic foreground and extragalactic sources. For the lensing maps, we adopt the publicly released masks, which both preserve about 70% of the sky. We stress that these masks largely account for the galactic dust emission and the carbon-monoxide lines (which may correlate to γ-ray foreground). In order to mitigate against multipole mixing, we further use an apodization over 5° for the *Planck* 2013 analysis. For the γ-ray maps, we prepare two masks combining the *Planck* 2013 lensing mask, a cut for galactic latitudes $|b| < 25°$, and excluding a 1° angular radius around each source in the 2 yr *Fermi*-LAT catalog (2FGL; Nolan et al. 2012) and the 4 yr *Fermi*-LAT catalog (3FGL; Fermi-LAT Collaboration et al. 2015), respectively. The 2FGL and 3FGL masks are apodized over 3° and 2°, respectively (the first choice being meant to provide us with a more conservative test), and the resulting effective sky fraction available is about 24% (2FGL) and 23% (3FGL). We explored different apodizations and sets of galactic masks (including larger galactic cuts and an additional mask for the region of the so-called "Fermi Bubbles"; Su et al. 2010), finding consistent results.

The cross-correlation APS between the *Planck* lensing map and the *Fermi*-LAT γ-ray map is estimated using a pseudo-C_ℓ approach (Hivon et al. 2002). To this aim, we make use of the publicly available tool PolSpice (Szapudi et al. 2001; Chon et al. 2004). Although the PolSpice algorithm properly deconvolves the signal APS from mask effects, it is known not to be a minimum variance algorithm (Efstathiou 2004). Thus, the associated covariance matrix is likely to be an overestimation of the actual uncertainty, and the significances reported throughout the paper can in turn be considered as conservative.

We bandpass filter the cross-correlation APS in the multipole range $40 < \ell < 400$ in order to reduce possible contamination from systematic effects. This multipole range was defined in Planck Collaboration et al. (2014b) as a confidence interval retaining 90% of the lensing information, with multipoles $\ell < 40$ requiring large mean-field bias corrections. Similarly, multipoles above a few hundred are hardly accessible with the *Fermi*-LAT sensitivity and angular resolution, and low multipoles correspond to the scales where the foreground cleaning has the largest impact (Fermi-LAT Collaboration et al. 2012a). Since the expected signal is predicted to scale as $1/\ell$ (see the next section), the analysis is performed in terms of $\ell\ C_\ell^{(\gamma\kappa)}$. In order to further mitigate mask mode-mixing, we average the APS in six linear bins of width $\Delta\ell = 60$.

First, we measure the cross-correlation APS between the CMB lensing and a single γ-ray map derived from the integrated counts at $E > 1$ GeV. A hint of a signal in the low-ℓ range (with a peak at $\ell \lesssim 150$–160) is present, while the larger-ℓ bins are compatible with no deviation from a null signal. We estimate the global significance of this low-ℓ peak evaluating the ratio of the measured APS over its error, $\langle \ell\ C_\ell^{\gamma_i\kappa}\rangle / \delta\langle \ell\ C_\ell^{\gamma_i\kappa}\rangle$, in three multipole-bins: $40 \leqslant \ell < 160$, $160 \leqslant \ell < 280$, and $280 \leqslant \ell < 400$. The errors are the diagonal elements of the covariance matrix obtained from PolSpice. We find the off-diagonal terms of the binned covariance matrix to be negligible. Considering the *Planck* 2015 map with a 3FGL mask (which is our reference analysis), the significances in the three multipole bins amount to 1.7, 0.0, and 0.2σ, respectively. The significance of the first bin for the four analyses arising from the combination of the Planck maps (2013 and 2015 releases) and the γ-ray point-source masks (2FGL and 3FGL) is reported in the first line of Table 1.

In order to better exploit all the available information encoded in the maps, we can combine the cross-correlation from the different γ-ray energy bins introduced above. Since the EGB spectrum roughly scales with $E^{-2.4}$ (see the inset in Figure 1), low-energy bins have larger statistics. On the other hand, the *Fermi*-LAT point-spread function significantly improves at high energy (Fermi-LAT Collaboration et al. 2012b). We therefore expect an information gain by splitting the signal in different energy bins. A minimum variance combination of the six single E-bin $C_b^{(\gamma^i\kappa)}$ measurements in a given multipole bin b can be defined as

$$C_b^{(\gamma\kappa)} = \sum_{i=1}^{6} w_i(b) C_b^{(\gamma^i\kappa)}, \quad w_i(b) = N_b \sum_{j=1}^{6} [\Gamma_b^{-1}]^{ij}, \qquad (1)$$

where $\Gamma_b^{ij} \equiv \mathrm{Cov}\left[C_b^{(\gamma^i\kappa)}, C_b^{(\gamma^j\kappa)}\right]$ is the 6×6 sub-matrix for the covariance in bin b, and $N_b = \left(\sum_{ij}\left[\Gamma_b^{-1}\right]^{ij}\right)^{-1}$. Note that after having checked the stability of our results against the inclusion of the correlation among different multipole bins $\Gamma_{bb'}^{ij}$, we choose not to include them for simplicity. We normalize $C_b^{(\gamma^i\kappa)}$ by means of the factor $E_i^{2.4}/\Delta E_i$ (with $E_i = \sqrt{E_{\mathrm{max},i} E_{\mathrm{min},i}}$ and $\Delta E_i = E_{\mathrm{max},i} - E_{\mathrm{min},i}$) to make it approximately flat in energy.

The computation of the full covariance matrix including correlation among different E-bins is not straightforward. Whereas the correlation terms among different multipole bins within an E-bin are provided by PolSpice, we estimate the off-diagonal correlation between the E_i and E_j bins (with $i \neq j$) using a two-step process. We first derive a semi-analytic

[6] http://fermi.gsfc.nasa.gov/ssc/data/access/lat/BackgroundModels.html

Table 1
Summary of Statistical Significances for the Three Adopted Methods

Energy		Multipole		Statistical Test	Significance			
					P15-3FGL	P15-2FGL	P13-3FGL	P13-2FGL
Single E-bin	[1, 300] GeV	Single ℓ-bin	$40 \leqslant \ell < 160$	$\langle \ell\, C_\ell^{\gamma\kappa}\rangle/\delta\langle \ell\, C_\ell^{\gamma\kappa}\rangle$	1.7σ	1.8σ	1.5σ	2.1σ
6 E-bins	[0.7, 300] GeV	Single ℓ-bin	$40 \leqslant \ell < 160$	$\langle \ell\, C_\ell^{\gamma\kappa}\rangle/\delta\langle \ell\, C_\ell^{\gamma\kappa}\rangle$	3.0σ	3.3σ	2.8σ	3.2σ
6 E-bins	[0.7, 300] GeV	6 ℓ-bins, $\Delta\ell = 60$	$40 \leqslant \ell < 400$	Model fitting	3.0σ	3.2σ	2.7σ	3.0σ

Notes. All analyses are performed on $\ell\, C_\ell^{\gamma\kappa}$ to make the observable approximately flat in multipoles. The errors $\delta\langle \ell\, C_\ell^{\gamma\kappa}\rangle$ are obtained from the covariance matrix of PolSpice. In the first row, the symbol $\langle\cdot\rangle$ denotes mean in the multipole bin. In the second row, the APS (and corresponding errors) at different energies E_i are obtained as discussed in connection to Equation (1) and are whitened through multiplication by $E_i^{2.4}/\Delta E_i$ (with the symbol $\langle\cdot\rangle$ denoting the average in a multipole bin and among energy bins). The third row reports model fitting: the significance is obtained from a χ^2 difference between the null signal and best-fit model. P15 (P13) stands for the analysis using the *Planck* 2015 (2013) map.

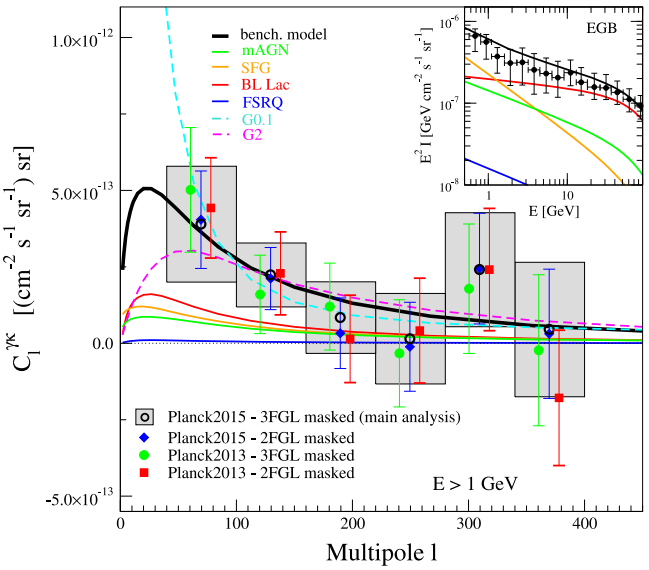

Figure 1. Cross-correlation APS $C_\ell^{(\gamma\kappa)}$ as a function of the multipole ℓ for γ-ray energies $E > 1$ GeV. The measurements are averaged (linearly in terms of $\ell\ C_\ell^{(\gamma\kappa)}$) in multipole bins of $\Delta\ell = 60$, starting at $\ell = 40$. Points report the minimum-variance combination of the measurement in individual energy bins (assuming a spectrum $\propto E^{-2.4}$), as described in Equation (1). Four different analyses are shown. They arise from the combination of two lensing maps (from *Planck* 2013 and 2015 releases) and two γ-ray point-source masks (2FGL and 3FGL). The benchmark theoretical model, shown in black, is the sum of the contributions from BL Lac objects (red), FSRQs (blue), mAGNs (green), and SFGs (orange), multiplied by $A^{\gamma\kappa} = 1.35$ (see the text). We also show two "generic" models, G0.1 and G2 with Gaussian $W(z)$ (normalized to provide the whole EGB above 1 GeV and then multiplied by the factor $A^{\gamma\kappa}$ described in the text), with peak at $z_0 = 0.1$ and width $\sigma_z = 0.1$ (cyan dashed), and $z_0 = 2$ and $\sigma_z = 0.5$ (magenta dashed), respectively. In the upper inset, we show the EGB benchmark model and *Fermi*-LAT measurement (Fermi-LAT Collaboration et al. 2014). The data used to create this figure are available.

Gaussian approximation (averaged in the multipole bin b):

$$\tilde{\Gamma}_b^{ij} = \left\langle \frac{C_\ell^{(\gamma^i\kappa)} C_\ell^{(\gamma^j\kappa)} + \boldsymbol{C}_\ell^{(\gamma^i\gamma^j)} \boldsymbol{C}_\ell^{(\kappa)}}{(2\ell + 1) f_{\rm sky}} \right\rangle_b , \qquad (2)$$

where $C_\ell^{(\gamma^i\kappa)}$ is the cross-correlation APS, estimated using a benchmark theoretical prediction discussed in the next section. (Note that this term is in any case subdominant in Equation (2).) $\boldsymbol{C}_\ell^{(\kappa)}$ and $\boldsymbol{C}_\ell^{(\gamma^i)}$ are the autocorrelation APS that we estimate from the corresponding maps using PolSpice and $\boldsymbol{C}_\ell^{(\gamma^i\gamma^j)}$ is the cross-correlation APS between the two energy bins i and j. As a sanity test, we checked that the noise-subtracted estimate $C_\ell^{(\gamma^i)} = \boldsymbol{C}_\ell^{(\gamma^i)} - \left(C_N^{(\gamma^i)} / W_\ell^2 \right)$ (where C_N is the power spectrum of the shot noise and W_ℓ is the beam function) agrees well with the autocorrelation APS reported by the Fermi-LAT Collaboration et al. (2012a). Similarly, our $\boldsymbol{C}_\ell^{(\kappa)}$ is consistent with theoretical expectations, once corrected for the noise APS provided in the *Planck* public data release (Planck Collaboration et al. 2014b). The factor $f_{\rm sky}$ corrects for the effective available fraction of the sky, but Equation (2) might actually underestimate the impact of masks. To have a more conservative error estimate, we derive a scaling coefficient $M_{i,b}$ from $\Gamma_b^{ii} = M_{i,b}^2\, \tilde{\Gamma}_b^{ii}$, where Γ_b^{ii} is obtained from PolSpice and $\tilde{\Gamma}_b^{ii}$ from Equation (2), and then we define the off-diagonal terms of the covariance matrix as $\Gamma_b^{ij} = M_{i,b} M_{j,b} \tilde{\Gamma}_b^{ij}$. The reliability of this scaling is further supported by the fact that we are using the same mask for all the γ-ray maps.

The combined APS $C_b^{(\gamma\kappa)}$ of Equation (1) is shown in Figure 1 for the four cases considered. Error bars are given by $\sqrt{N_b}$. The different analyses are in excellent agreement with each other. As for the analysis with gamma-rays integrated above 1 GeV, we estimate the significance of the cross-correlation signal in the multipole-bins $40 \leqslant \ell < 160$, $160 \leqslant \ell < 280$, and $280 \leqslant \ell < 400$. The significances now amount to 3.0, 0.7, and 1.2σ, respectively. A comparison with the results of the previous analysis shows that by adding spectral information increases the significance of the signal in the low-ℓ sector, while in the larger-ℓ bins the cross-correlations are still compatible with zero. The results obtained so far therefore show evidence of correlation for multipoles below $\ell \lesssim 150$–160.

As a cross-check for the stability of the γ-ray data, we repeat the analysis considering the data from the first 150 weeks and subsequent 150 weeks separately. The obtained APS are compatible and, once combined together, very closely resemble the APS of the full period presented above.

The subtraction of the galactic foreground in the γ-ray maps has a significant systematic uncertainty related to the modeling of the galactic diffuse emission, which can affect anisotropies on large scales (Fermi-LAT Collaboration et al. 2012a). The foreground residuals in the lensing map are instead thought to

be more under control since they do not show up in the autocorrelation studies (Planck Collaboration et al. 2015). Assuming the lensing map to be free from galactic contaminations, the presence of a gamma-ray galactic foreground in the maps would not provide a cross-correlation signal. Rather, it would only act as a noise term. To test this, we performed the same analysis discussed above but employed γ-ray maps where the foreground was not subtracted. We found the same central values for the cross-correlation APS points, but with larger errors (and so lower statistical significance), consistent with the fact that the galactic foregrounds contribute to the error budget but not to the signal. This suggests that possible contaminations of the APS from a galactic foreground bispectrum are small.

In the next section, we will show that the derived APS can be explained in terms of gamma-ray emission from astrophysical sources emitting mostly at intermediate redshifts.

3. INTERPRETATION

We now move on to discuss the agreement between theoretical models and the measurements reported in Figure 1.

In the Limber approximation (Limber 1953), the theoretical two-point cross-correlation APS can be computed as

$$C_\ell^{(\gamma\kappa)} = \int \frac{d\chi}{\chi^2} W_\gamma(\chi) W_\kappa(\chi) P_{\gamma\kappa}(k = \ell/\chi, \chi). \quad (3)$$

where $\chi(z)$ denotes the radial comoving distance, W_κ and W_γ are the window functions for lensing and γ-rays, and $P_{\gamma\kappa}$ is the three-dimensional power spectrum (PS) of the cross-correlation. For the latter, we follow the halo model approach (see, e.g., Cooray & Sheth 2002 for a review), where P can be split into one-halo P_{1h} and two-halo P_{2h} components as $P = P_{1h} + P_{2h}$ (see Fornengo & Regis 2014 for their expressions).

The CMB lensing window function is given by (Bartelmann 2010)

$$W_\kappa(\chi) = \frac{3}{2} H_0^2 \Omega_m [1 + z(\chi)] \chi \frac{\chi_* - \chi}{\chi_*}, \quad (4)$$

where H_0 is the Hubble constant, Ω_m is the matter-density parameter, and χ_* is the comoving distance to the last-scattering surface.

The window function for a γ-ray emitter i is (see, e.g., Camera et al. 2013)

$$W_{\gamma_i}(E, z) = \frac{\int_{\mathcal{L}_{\min}(z)}^{\mathcal{L}_{\max}(z)} d\mathcal{L}\ \Phi_{\gamma_i}\mathcal{L}}{4\pi(1+z)} \exp[-\tau[E(1+z), z]], \quad (5)$$

where $\mathcal{L}$ is the γ-ray luminosity per unit energy range, $\Phi_\gamma(\mathcal{L}, z)$ is the γ-ray luminosity function (GLF), and τ is the optical depth for absorption (Stecker et al. 2007).

We consider four different extragalactic γ-ray populations: star-forming galaxies (SFGs), misaligned AGNs (mAGNs), and two subclasses of blazars, BL Lacertae objects (BL Lac objects) and flat-spectrum radio quasars (FSRQs). The GLFs of the last three source classes are taken from the best-fit models of Di Mauro et al. (2014), Ajello et al. (2014), and Ajello et al. (2012), respectively. In the case of SFGs, we consider the infrared luminosity function from Gruppioni et al. (2013; adding up spiral, starburst, and SF-AGN populations of their Table 8), and linking γ and infrared luminosities by means of the relation derived in Fermi-LAT Collaboration et al. (2012c). The energy spectrum is assumed to be a power law with spectral indexes −2.7 (SFGs), −2.37 (mAGNs), −2.1 (BL Lac objects), and −2.4 (FSRQs). The model fairly reproduces *Fermi*-LAT measurements for both the EGB (see the upper right inset of Figure 1) and the γ-ray autocorrelation APS. For the latter, we found a flat APS (given by the one-halo term and dominated by BL Lac object contribution) of $C_\ell = 1.5 \times 10^{-17}\,\mathrm{cm^{-4}\,s^{-2}\,sr^{-1}}$ for $E > 1\,\mathrm{GeV}$.

The cross-correlation power spectrum at the intermediate scales considered here is mostly set by the linear part of the clustering, $P \simeq P_{2h}$, which is similar in the various cases (i.e., it is related to the linear total matter PS P_{lin}), except for the specific bias term, with negligible contribution from P_{1h}. In other words, we approximately have $C_\ell^{(\gamma_i)\kappa} = \int d\chi\ \chi^{-2}\ W_{\gamma_i}(\chi) W_\kappa(\chi) b_{\rm eff}^{\gamma_i}(z) P_{\rm lin}(\ell/\chi, \chi)$, where the "effective" bias of a γ-ray population is $b_{\rm eff}^{\gamma_i}(z) = \int d\mathcal{L}\ b^{\gamma_i}(\mathcal{L}, z) \Phi_{\gamma_i}\mathcal{L} / \left(\int d\mathcal{L}\ \Phi_{\gamma_i}\mathcal{L} \right)$, with $b^{\gamma_i}(\mathcal{L}, z)$ being the bias between the γ-ray source i and matter, as a function of luminosity and redshift. To estimate the latter, we use the halo bias b_h (Sheth & Tormen 1999; setting $b^{\gamma_i}(\mathcal{L}, z) = b_h\left(M^{\gamma_i}(\mathcal{L}, z)\right)$ and the relation $M^{\gamma_i}(\mathcal{L}, z)$ (setting the mass of the halo hosting astrophysical object i with a certain luminosity), as described in Camera et al. (2014). Comparing the bias of blazars obtained in our analysis with the bias derived in Allevato et al. (2014), we find the latter to be somewhat larger than our estimates. We obtain a mean mass hosting the object of $M = 5 \times 10^{12}$ (BL Lac objects) and $M = 1.5 \times 10^{13} M_\odot$ (FSRQs) contrary to $M = 3 \times 10^{13} M_\odot$ of Allevato et al. (2014). However, our measurement probes the unresolved (individually fainter) component that resides in less massive halos than the brightest blazar subsample considered in Allevato et al. (2014). Thus, the two results are not in contradiction.

The cross-correlation APS predicted in the models of the four γ-ray emitters described above and their collective contribution are shown in Figure 1.

With the theoretical model at hand, we can fit its overall amplitude $A^{\gamma\kappa}$ by minimizing the χ^2, which is computed by means of the full covariance matrix introduced above. The statistical significance of the model is derived computing the $\Delta\chi^2$ between the null signal and best-fit model. We obtain $A^{\gamma\kappa} = 1.35 \pm 0.45$ with 3.0σ significance, which shows a statistically significant preference for a signal with the correct features expected from the extragalactic gamma-ray emission.

The window functions of the considered γ-ray populations are all peaked at $z \sim 0.5$–1. To explore in a more general way the kind of γ-ray model preferred by the data, we compute in Figure 1 the signals from two Gaussian window functions $W(z) \propto \exp\left[-(z - z_0)/\sigma_z^2\right]$: one peaked at low redshift (model G0.1 with $z_0 = \sigma_z = 0.1$), one peaked at high redshift (model G2 with $z_0 = 2$ and $\sigma_z = 0.5$), and both normalized to match the *Fermi*-LAT EGB measurement above 1 GeV (and bias modeled as for mAGNs). We find $A_{G0.1}^{\gamma\kappa} = 2.99 \pm 0.96$ (3.1σ) and $A_{G2}^{\gamma\kappa} = 0.85 \pm 0.29$ (2.9σ). For $W(z)$ peaked at $z \gg 1$, the relative contribution of small (more distant) objects with respect to larger objects increases, while no power is detected at small scales (above $\ell \sim 150$). This slightly reduces the statistical significance (although with the current data accuracy we cannot exclude this possibility). On the contrary, $W(z)$ peaked at low z would provide the right bump at low ℓ,

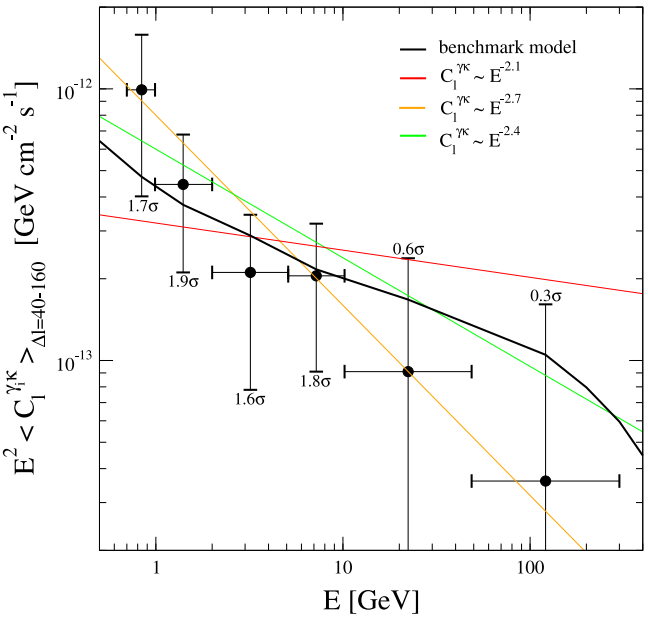

Figure 2. Energy dependence of the cross-correlation APS. The reported points are for $E^2 \langle C_\ell^{\gamma_i\kappa} \rangle_{\Delta\ell=40-160}$, which is the energy-differential APS of each energy bin i averaged in the multipole bin $40 < \ell < 160$ and multiplied by E^2. Errors are from the diagonal of the covariance matrix, and we report the statistical significance of each point. The benchmark theoretical model is shown in black and is multiplied by the energy-averaged amplitude $A^{\gamma\kappa} = 1.35$.

increasing the statistical significance. However, the large value of the overall amplitude translates into $\langle b_{\rm eff} \rangle \sim 3$, which is typically way too large for a low-z population (see, e.g., Cooray & Sheth 2002). Note also that since the window function of the CMB lensing peaks at moderately high redshift, as mentioned in the Introduction, its overlapping is more effective with high-z γ-populations rather than low-z emitters. Therefore, in the latter case, the required $\langle b_{\rm eff} \rangle$ becomes slightly larger.

The above arguments seem to suggest that in order to reproduce the observed cross-correlation, the bulk of γ-ray contribution to the EGB have to reside at intermediate redshift.

Figure 2 shows the measured cross-correlation APS for different energy bins and averaged in the multipole bin $40 < \ell < 160$. The spectrum is consistent with the benchmark model and similar to the *Fermi*-LAT EGB spectrum (having a spectral index close to −2.4), although possibly slightly softer.

4. DISCUSSION AND CONCLUSIONS

We reported the first indication of a cross-correlation between the unresolved γ-ray sky and CMB lensing. The analysis also points toward direct evidence that the IGRB is of extragalactic origin. The analysis has been based on the γ-ray data of the first 68 months of operation of the *Fermi*-LAT and on the 2013 public release by the *Planck* Collaboration of the CMB lensing potential map. Current models of AGNs and SFGs can fit well the amplitude, angular dependence, and energy spectrum of the observed APS. The size of the signal appears to be robust against variations of the analysis assumptions. Data exhibit a preference for a signal with the correct features expected from the extragalactic gamma-ray emission with a 3.0σ significance.

The forthcoming *Fermi*-LAT Pass-8 reprocessed events will allow for a more refined assessment of the signal. Moreover, the technique presented in this work can be also applied for cross-correlating the γ-ray sky with probes of the large-scale structure of the universe at different redshifts (such as galaxy catalogs and weak-lensing surveys). Such a tomographic analysis of the EGB will provide invaluable information about its composition.

Contaminations from foreground, either real (e.g., a dust or point-source bispectrum) or spurious, cannot, at present, be totally excluded, but they are significantly disfavored. A model of γ-ray populations built to explain the EGB, and not tuned to the measurement presented here, matches the data well both in features and normalization. More generically, a population of extragalactic γ-ray emitters following matter clustering at large scales with GLF peaked at intermediate z and with $\langle b_{\rm eff} \rangle \sim 2$–3 agrees well with the data, once the associated EGB is normalized to fit the *Fermi*-LAT measurement of the IGRB. On the contrary, if, for example, the contribution to the IGRB is reduced to 50%, the required bias would become $\langle b_{\rm eff} \rangle \sim 4$–6, which is likely unrealistically large. This implies that the presented results can be considered as first direct proof that the majority of the IGRB is emitted by extragalactic structures.

We thank D. Maurin for a question that was the actual kickoff of the project and A. Cuoco, M. Fornasa, and H. Zechlin for insightful discussions. This work is supported by the research grant *Theoretical Astroparticle Physics* number 2012CPPYP7 under the program PRIN 2012 funded by the Ministero dell'Istruzione, Università e della Ricerca (MIUR), by the research grants *TAsP* (*Theoretical Astroparticle Physics*) and *Fermi* funded by the Istituto Nazionale di Fisica Nucleare (INFN), and by the *Strategic Research Grant: Origin and Detection of Galactic and Extragalactic Cosmic Rays* funded by Torino University and Compagnia di San Paolo.

REFERENCES

Ajello, M., Shaw, M. S., Romani, R. W., et al. 2012, ApJ, 751, 108
Ajello, M., Romani, R. W., Gasparrini, D., et al. 2014, ApJ, 780, 73
Allevato, V., Finoguenov, A., & Cappelluti, N. 2014, ApJ, 797, 96
Ando, S. 2014, JCAP, in press (arXiv:1407.8502)
Ando, S., Benoit-Lèvy, A., & Komatsu, E. 2014, PhRvD, 90, 023514
Bartelmann, M. 2010, CQGra, 27, 233011
Blanchard, A., & Schneider, J. 1987, A&A, 184, 1
Camera, S., Fornasa, M., Fornengo, N., & Regis, M. 2013, ApJL, 771, L5
Camera, S., Fornasa, M., Fornengo, N., & Regis, M. 2014, arXiv:1411.4651
Chon, G., Challinor, A., Prunet, S., Hivon, E., & Szapudi, I. 2004, MNRAS, 350, 914
Cooray, A., & Sheth, R. 2002, PhR, 372, 1
Di Mauro, M., Calore, F., Donato, F., Ajello, M., & Latronico, L. 2014, ApJ, 780, 161
Efstathiou, G. 2004, MNRAS, 349, 603
Fermi-LAT Collaboration, Abdo, A. A., Ackermann, M., Ajello, M., et al. 2010, PhRvL, 104, 101101
Fermi-LAT Collaboration, Acero, F., Ackermann, M., Ajello, M., et al. 2015, ApJS, submitted (arXiv:1501.02003)
Fermi-LAT Collaboration, Ackermann, M., Ackermann, M., Ajello, M., Albert, A., et al. 2012a, PhRvD, 85, 083007
Fermi-LAT Collaboration, Ackermann, M., Ackermann, M., Ajello, M., Albert, A., et al. 2012b, ApJS, 203, 4
Fermi-LAT Collaboration, Ackermann, M., Ackermann, M., Ajello, M., Allafort, A., et al. 2012c, ApJ, 755, 164
Fermi-LAT Collaboration, Ackermann, M., Ackermann, M., Ajello, M., et al. 2014, ApJ, in press (arXiv:1410.3696)
Fornengo, N., & Regis, M. 2014, FrPhy, 2, 6
Gruppioni, C., Pozzi, F., Rodighiero, G., et al. 2013, MNRAS, 432, 23

Hivon, E., Górski, K. M., Netterfield, C. B., et al. 2002, ApJ, 567, 2
Lewis, A., & Challinor, A. 2006, PhR, 429, 1
Limber, D. N. 1953, ApJ, 117, 134
Nolan, P. L., Abdo, A. A., Ackermann, M., et al. 2012, ApJS, 199, 31
Okamoto, T., & Hu, W. W. 2003, PhRvD, 67, 083002
Planck Collaboration, Ade, P. A. R., Aghanim, P. A. R., Armitage-Caplan, C., et al. 2014a, A&A, 571, A16
Planck Collaboration, Ade, P. A. R., Aghanim, P. A. R., Armitage-Caplan, C., et al. 2014b, A&A, 571, A17
Planck Collaboration, Ade, P. A. R., Aghanim, P. A. R., Arnaud, M., et al. 2015, arXiv:1502.01591
Sheth, R. K., & Tormen, G. 1999, MNRAS, 308, 119
Shirasaki, M., Horiuchi, S., & Yoshida, N. 2014, PhRvD, 90, 063502
Stecker, F. W., Malkan, M. A., & Scully, S. T. 2007, ApJ, 658, 1392
Su, M., Slatyer, T. R., & Finkbeiner, D. P. 2010, ApJ, 724, 1044
Szapudi, I., Prunet, S., & Colombi, S. 2001, ApJL, 561, L11
Xia, J.-Q., Cuoco, A., Branchini, E., Fornasa, M., & Viel, M. 2011, MNRAS, 416, 2247